We are IntechOpen, the world's leading publisher of Open Access books Built by scientists, for scientists

6,900
Open access books available

185,000
International authors and editors

200M
Downloads

Our authors are among the

154
Countries delivered to

TOP 1%
most cited scientists

12.2%
Contributors from top 500 universities



WEB OF SCIENCE™

Selection of our books indexed in the Book Citation Index in Web of Science™ Core Collection (BKCI)

Interested in publishing with us?
Contact book.department@intechopen.com

Numbers displayed above are based on latest data collected.
For more information visit www.intechopen.com



Chapter 3

Birefringence in Photonic Crystal Structures: Toward Ultracompact Wave Plates

Wenfu Zhang and Wei Zhao

Additional information is available at the end of the chapter

http://dx.doi.org/10.5772/55142

1. Introduction

Birefringence is an important optical effect of materials that having different refractive indices for different polarizations of light. Birefringence and related optical effects play an important role in quantum and nonlinear processes and also have been widely used in modern optical devices, such as optical sensors, light modulators, liquid crystal displays, crystal filters, medical diagnostics, and wave plates (WPs). Among these, WP is one of the most essential elements in many optical modules and equipment, and will certainly have many applications in future photonic integrated circuits (PICs).

According to the difference of generation mechanism, birefringence could be divided into two types: natural birefringence and artificial birefringence, which are microscopic and macroscopic anisotropy induced, respectively [1]. Generally, artificial birefringence is larger than natural birefringence and has designable characteristics. Many artificial structures with high birefringence have been proposed and studied recently. Table 1 gives the comparison of birefringence, dispersion and loss of different structures containing multilayer film (MF) [2], nanowires (NW) [3], metamaterials (MM) [4], plasmonic nanoslits array (PNA) [1], multi-slotted dielectric waveguides (MSDW) [5], bulk photonic crystal (PhC) [6-8], two dimensional (2D) PhC waveguide (PhCW) [9, 10], and periodic dielectric waveguide (PDW) which also named as one dimensional (1D) PhCW [11, 12]. Among these artificial materials, the PhC related structures are more important not only for the excellent birefringence properties but also the great importance of PhC in PICs.

PhCs are structures with periodic arrangement of dielectrics or metals, which provide the ability of molding the flow of light in it [13-15]. Due to the unique guiding properties of PhC structure, such as the photonic band gap guidance, it is foreseen as one of the key artificial materials for next generation PICs. This chapter gives a thorough review of the birefringence

INTECH
open science | open minds

© 2013 Zhang and Zhao; licensee InTech. This is an open access article distributed under the terms of the Creative Commons Attribution License (http://creativecommons.org/licenses/by/3.0), which permits unrestricted use, distribution, and reproduction in any medium, provided the original work is properly cited.

properties of PhC structures containing 1D PhCW (PDW), 2D PhCW and bulk PhC. The applications of the giant birefringence of PhC structures in both low-order WPs and high-order WPs are studied in details. This chapter is organized as follow. In Sec. 2, an overview of numerical algorithms used in this chapter is given. In Sec. 3, the birefringence properties are studied taking 2D PhCWs, 2D bulk PhCs, and 1D PhCWs as examples. High performance WPs are designed based on different PhC structures in Sec. 4. Discussions and conclusions are given in Sec. 5.

	MF	NW	MM	PNA	MSDW	PhCW	Bulk PhC	PDW
Δn	~0.3	~0.8	~3.2	2.7	1.0	0.111	0.938	1.5
Achromatic	-	-	No	No	-	Yes	Yes	Yes
Loss	Low	-	High	High	Low	Low	High	Low

* This table is from reference [12]

Table 1. Birefringence of different artificial structures

2. Numerical algorithms

Many numerical algorithms which solve the partial differential equations can be used in computational photonics. For PhCs, two categories of problems are most important [15]: one is frequency-domain eigenvalue problem which refers to find the band structure ω(k) and associated electromagnetic fields; the other one is time-domain calculation which is related to obtain the fields E(x, t) and H(x, t) propagating in time. For the frequency-domain eigenproblems, plane wave expansion method (PWE) is the most popular method to get the dispersion relation (band structure) of specific PhC geometries [15, 16]. Correspondingly, Finite-difference time-domain method (FDTD) [17, 18] is the most important time-domain simulation approach for PhCs to get the propagating fields and transmission/reflection spectrum.

2.1. Plane Wave Expansion method (PWE)

PWE is used to solve the Maxwell equations by formulating an eigenvalue problem. The master equation for PhCs can be deduced from Maxwell equations as follow:

$$\hat{\Theta}\mathbf{H}(\mathbf{r}) = \left(\frac{\omega}{c}\right)^2 \mathbf{H}(\mathbf{r}) \tag{1}$$

http://dx.doi.org/10.5772/55142

where ω is angular frequency, c is the vacuum speed of light, r is the position vector, and H(r) is the macroscopic magnetic field. $\hat{\Theta}$ is a linear Hermitian operator and $\hat{\Theta}H(r)$ is written as [15]

$$\hat{\Theta}\mathbf{H}(\mathbf{r}) = \nabla \times \left(\frac{1}{\varepsilon(\mathbf{r})} \nabla \times \mathbf{H}(\mathbf{r}) \right) \tag{2}$$

where ε(r) is the relative permittivity of dielectric materials. By using the plane wave basis, the Bloch eigenmodes and band structures of the perfect periodic structures could be easily obtained by solving the master equation. However, for the non-periodic or quasi-periodic structures, such as line defect PhCWs, and the structures without periodically in all dimensions, the supercell technique must be used by choosing a large computational cell as the periodic element which helps to get the isolated electromagnetic modes. By using the supercell method, both point and line defect modes of PhCs can be solved. Taking a PhCW as example, the structure is square lattice dielectric rods in air. The radius of the dielectric rods is r=0.2a, where a is the lattice constant, and the permittivity is ε=8.9. The line defect is introduced by removing one row of dielectric rods in the ΓX direction. Fig. 1 gives the dispersion curves calculated by supercell method. The square lattice PhCW has single transverse-magnetic (TM) guided mode in the normalized frequency range of 0.32-0.446 a/λ, which locates in the photonic band gap (PBG) range of TM polarization mode. This reveals that the PhCW has PBG guided TM mode but no guided mode for TE polarization.

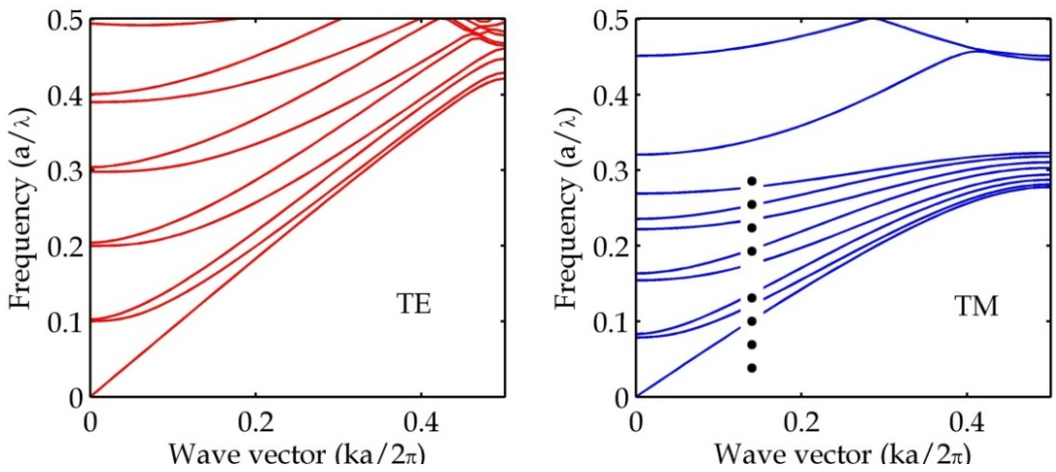


Figure 1. Dispersion curves of line defect square lattice PhCW. The inset is the 1×9a supercell used in PWE calculations. The parameters of the PhCW are chosen as follow: permittivity of high and low index materials are ε_H=8.9 and ε_L=1, respectively and the radius of dielectric rods is r=0.2a.

The PWE is suitable to calculate the band structure of PhC, but not conventional to get the transmission spectra of PhC. When the loss and transmitting properties of PhC are required, FDTD method is often used for the advantages of that broadband response can be accurately obtained in only one simulation run.

2.2. Finite-Difference Time-Domain method (FDTD)

The FDTD method is one of the grid-based differential time-domain numerical modeling methods. The time-derivative parts of Maxwell equations in partial differential form are written:

$$\begin{aligned} \frac{\partial \mathbf{B}}{\partial t} &= -\nabla \times \mathbf{E} - \mathbf{J}_B \\ \frac{\partial \mathbf{D}}{\partial t} &= -\nabla \times \mathbf{H} - \mathbf{J} \end{aligned} \tag{3}$$

where B is the electric displacement, D is the magnetic induction fields, J is the electric-charge current density, and J_B is an imaginary magnetic-charge current density for calculation convenience. By central-difference approximations, e.g. standard Yee grid [19], the electric and magnetic fields governed by Eq. (3) are discretized both in time and space. By properly selecting of initial excitation current J or J_B, the resulting finite-difference equations are solved in a leapfrog manner: the electric field vector components in a volume of space are solved at a given instant of time; then the magnetic field vector components in the same spatial volume are solved at the next instant of time; and the process is repeated over and over again until the desired transient or steady-state electromagnetic field behavior is fully evolved.

Although a lot of FDTD solver packages are available in literature, we use the free software MEEP [18] which is developed by MIT's researchers in this chapter. The transmission spectrum of PhC structures can be easily obtained by the FDTD solver. Still take the square lattice PhCW studied in Fig. 1 as example, the transmission spectrum for the TM polarization of the PhCW with length of 27*a* is shown in Fig. 2. From the figure, the PhCW is low loss in the frequency range of 0.32-0.446 a/λ which is consistent with the simulation results taken by PWE method.

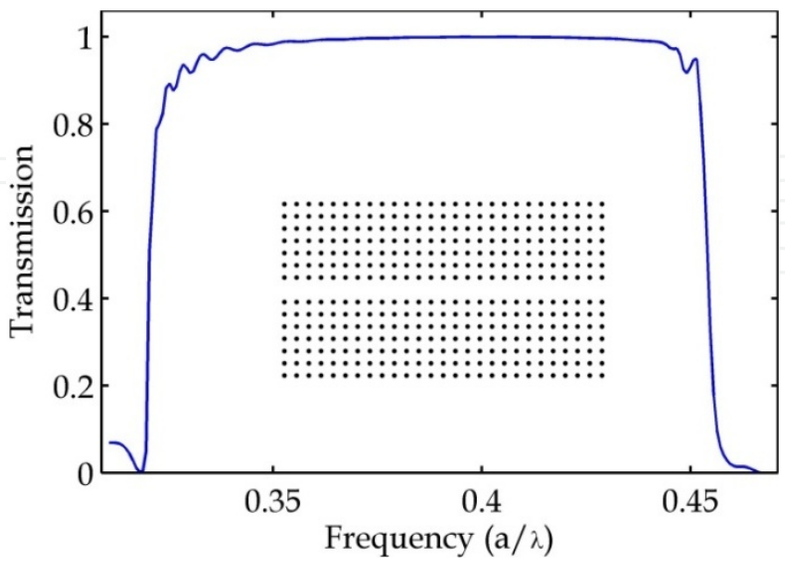


Figure 2. Transmission spectrum for the TM mode of the line defect square lattice PhCW. The inset is the PhCW structure used in FDTD simulation and the parameters of PhCW are as same as that in Fig. 1.

2.3. Spatial Fourier Transform method (SFT)

Except for the low loss of the PhC structures, large birefringence is essential for realizing the ultracompact WPs. The frequency-dependent effective mode indices for both TE and TM modes of PhC structure should be calculated to obtain the birefringence of the structures. When the PhC structure has single mode in the operating frequency range, such as PBG guided TM mode, in the PhCW shown in Fig. 1, the mode indices can be obtained from the dispersion curves calculated by PWE method. But, for the PhC structures with quasi-periodic and non-periodic structures or some special PhCW without PBG guided modes but total internal reflection (TIR) modes, the dispersion curves of the guided modes are difficultly obtained by the conventional PWE method. In this chapter, the SFT method [20] is used when the birefringence of this category of structure needs to be calculated.

The SFT method is based on the spatial Fourier transform spectrum of the electromagnetic field distributions of the waveguide mode along the propagating direction. Assuming $u_\omega(x, y_0)$ is the field distribution of waveguide mode at the given plane $y=y_0$ along the propagating direction x, where u is E or H, ω is the angular frequency of the mode, x is the propagation direction, and y is the direction perpendicular to x in the plane. The field can be expanded by the plane wave basis as $u_\omega(x, y_0) = \sum_n u_{n,\omega} \exp(j\beta_{n,\omega} x)$, where $u_{n,\omega}$ and $\beta_{n,\omega}$ are the field component and the propagation constant of the nth mode at frequency ω, respectively. The propagation constant $\beta_{n,\omega}$ can be extracted from the peaks of the SFT spectrum of $u_\omega(x, y_0)$. For the Bloch mode of the periodic structure, the wavevector β still can be obtained from the SFT analysis for that the peaks of SFT spectrum always located at $\beta+m(2\pi/a)$, where m is an integer [20].

To verify the SFT method, the field distribution of TM mode in the PhCW studied in Fig. 1 and Fig.2 are calculated by FDTD method and the snapshot of E_z fields at the frequency of 0.40 a/λ is shown in Fig. 3 (a). The peak of the SFT spectrum (as shown in Fig. 3 (b)) is located at $0.292\, a/2\pi$ which is as same as the Bloch wave vector obtained by PWE methods. The dispersion diagrams obtained by PWE and SFT method in frequency range of 0.34-0.42 a/λ are almost same as shown in Fig. 3 (c), which shows the validity of the SFT technique in the mode calculation for the PhCW structures.

3. Birefringence of PhC structures

Birefringence is related to the effective index difference of two orthogonal polarization modes and can be expressed as $\Delta n = n_p - n_s$, where p and s are TE (TM) and TM (TE), respectively, in this chapter. It is the basis on which the ultracompact WP is realized. Fortunately, most of the PhC structures have large birefringence for the large index difference of the composed materials of PhCs. Researching results show that the 2D PhCW having birefringence of ~0.07 and ~0.1 for square and triangular lattice air holes in high index materials, respectively [10]. For the 2D bulk PhCs, experimental results reveal that the birefringence is as high as 0.2 [8], and the theoretical analysis results are higher. The 1D PhCWs give giant birefringence which is higher than 1 [12]. In this section, the birefringence properties of different PhC structures, containing 2D PhCW, 2D bulk PhC and 1D PhCW, will be reviewed in details.

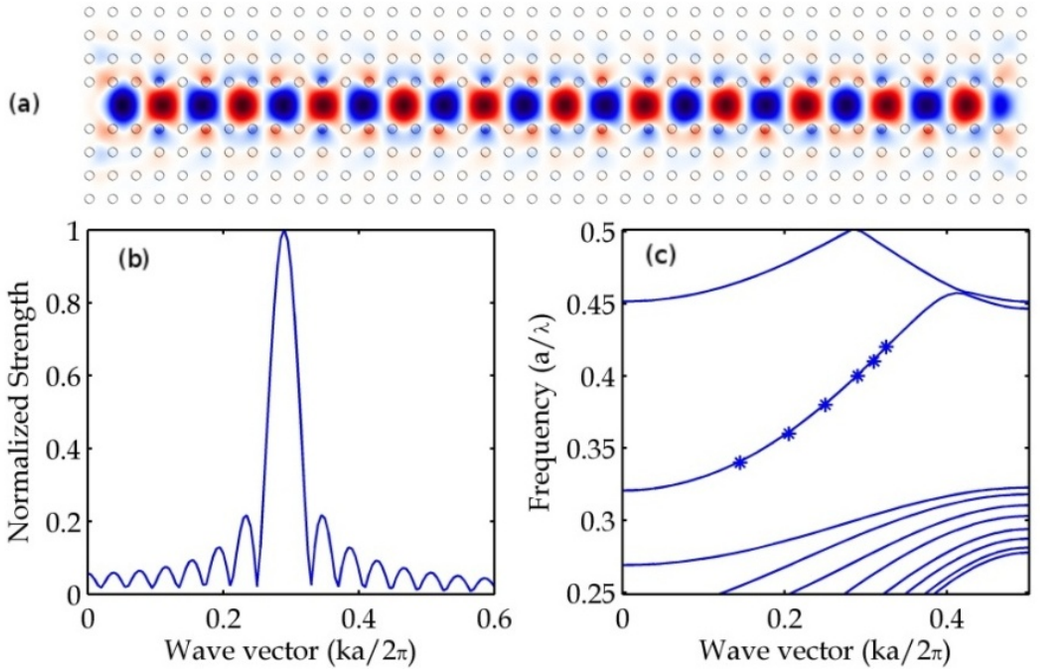


Figure 3. The snapshot of E_z field distribution for the TM guided mode of the square lattice PhCW at frequency of 0.40 a/λ; (b) SFT spectrum of the E_z field shown in (a); (c) Dispersion curves (also shown in Fig. 1) of the TM polarization, the solid lines are obtained by PWE method and the stars represent the results calculated by the SFT method.

3.1. Birefringence of 2D PhCW

For birefringence related applications, both TE and TM polarized light must propagate with low loss in the 2D PhCW which is formed by introducing of line defect in the perfect bulk PhC at a given direction. Different guided mechanisms could be used to confine light in the 2D PhCWs [21]. The widely studied mechanism in the literature is the PBG guiding as that shown in Fig. 1. It is difficult to realize 2D PhCW supporting both TE and TM PBG guided modes, only if carefully choosing the materials and geometry structures. Studied results show that the 2D PhCW can also guide the light as that in the conventional dielectric slab waveguide by total internal refection (TIR) guiding mechanism. Compound of PBG and TIR effects could also make low loss guiding for both TE and TM mode in the 2D PhCW [21-23].

3.1.1. Birefringence of 2D PhCW with PBG guided modes

The PhCW with hybrid triangular and honeycomb lattices can support both TE and TM modes [24, 25]. The structure is shown in Fig. 4 and has been optimized as follow: The permittivity of the background high index material is 11.56, and the radii of the large and small air holes are r_1=0.27$_a$ and r_2=0.15$_a$, respectively. The waveguide is formed by a line defect of elliptical air holes with major and minor axes of d_a=0.4$_a$ and d_b=0.2$_a$, respectively. Two lines of small air holes with radius of r_2 are added to get single TE and TM propagation.

http://dx.doi.org/10.5772/55142

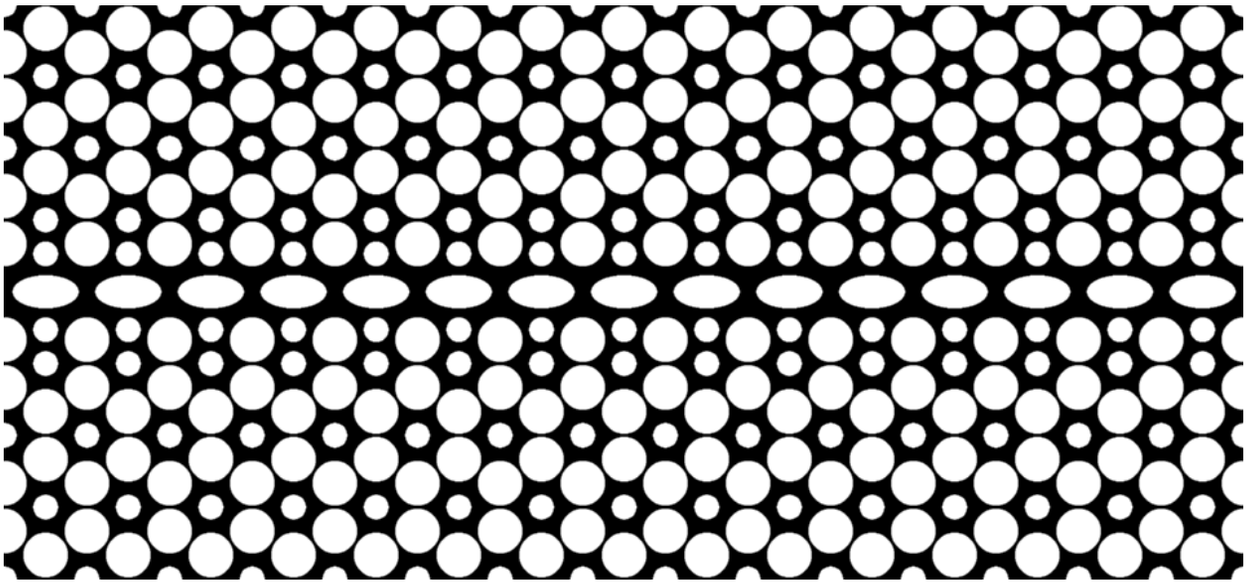


Figure 4. The structure of PhCW with hybrid triangular and honeycomb lattices, which supports PBG guided TE and TM modes. [24, 25]

The band structure of PhCW shown in Fig. 4 is calculated by PWE method with $1\times4\sqrt{3}a$ supercell as shown in Fig.5 (a) [24]. The single TE and TM mode region is 0.558-0.569 a/λ, which located in the absolute band gap of the bulk PhC. The effective indices of the TE and TM modes are obtained from the dispersion curves and the birefringence Δn in the single mode region are calculated and shown in Fig. 5 (b). The birefringence can be larger than 0.5, which is much higher than the natural birefringence in the birefrigenct crystals. However, the structure has large dispersion for that the birefringence varies from 0.2 to 0.56 in the operating frequency region.

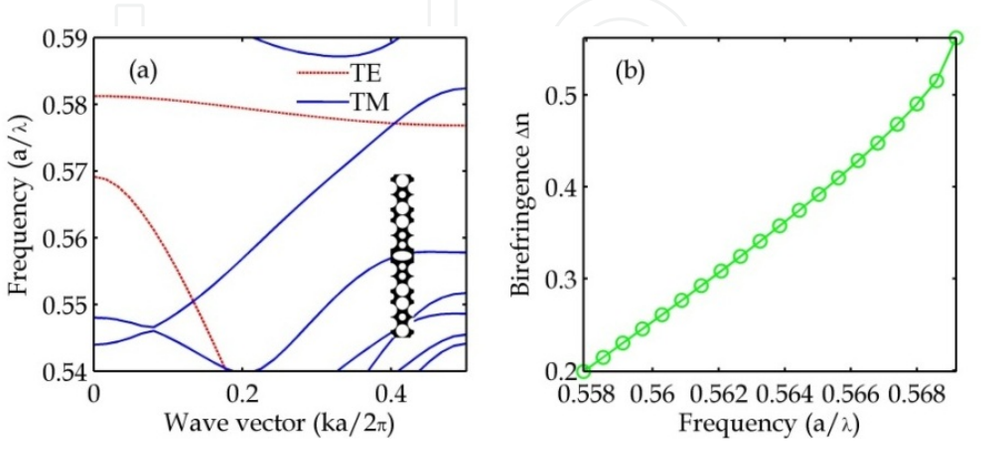


Figure 5. (a) Dispersion curves of PhCW shown in Fig. 4. The inset is the supercell used in PWE calculations. (b) Birefringence (Δn) of PhCW in the single mode region.

3.1.2. Birefringence of 2D PhCW with hybrid PBG and TIR guided modes

The PhCWs with both square and triangular lattice air holes in high index materials can support low loss transmitting of TE and TM polarizations with the help of TIR guided mechanism [21-23]. Taking a square lattice PhCW as example, the waveguide is formed by introducing of a line defect in ΓX direction in the perfect PhC which has square lattice air holes in high index material with permittivity of 12.96. Calculated dispersion curves of the PhCW are shown in Fig. 6 for both TE and TM polarizations. The PhCW has single TE guided mode in the normalized frequency range of 0.248-0.272a/λ, which locates in the PBG region of TE polarization mode. This reveals that the PhCW has PBG guided TE mode. However, there are no PBG guided modes in this frequency range for TM polarization as shown in Fig. 6 (b). To fully understand the guiding properties of the PhCW, the transmission spectra for both TE and TM polarization of the PhCW with length of 21a are calculated by FDTD method and shown in Fig. 7 (a). New information could be obtained from the figure: 1) Wider frequency range for low-loss guiding TE mode is achieved which reveals that the guiding mechanisms of the TE mode are not only PBG but also TIR; 2) Although there is no band-gap for TM mode in the frequency range of 0.24-0.30 a/λ, the TM polarization also can propagate with low-loss in this frequency range by the TIR mechanism. From the insets of Fig. 7 (a), EM fields are confined well in the line defect waveguide region for both TE and TM polarizations. For the effective indices of TM guided modes can't be obtained directly from the dispersion curves calculated by the PWE method, the SFT method is used to study the birefringence properties of the PhCW with hybrid PBG and TIR guided modes. By launching the continuous wave (CW) source with single frequency in the low loss frequency range of 0.255-0.268 a/λ, the EM field distributions for the guided mode of both TE and TM polarization are calculated by FDTD method. The propagation constants of guided modes, which are used to the calculating of effective indices, are found by seeking the peaks of the SFT spectra of the EM fields. Fig. 7 (b) shows the birefringence property of the 2D square lattice PhCW with hybrid PBG and TIR guided modes. The birefringence of the 2D square lattice PhCW is much lower than that shown in Fig. 5 (b), however, the PhCW has advantages of easily design and high tolerance of distortion in fabrication. Except for the square lattice structure, the PhCW with triangular lattice air holes in high index material is also can be used as birefringent waveguide for the WP applications. Previously studied results shows that the birefringence in the triangular lattice PhCW is a little higher than that in the square lattice structures [10].

3.2. Birefringence of 2D bulk PhCs

Actually, the typical bulk PhC itself is strongly anisotropic artificial material which provides large birefringence. Different from the PhCW, the PhC as birefringent media must work outside the PBG for that the PhC are highly reflection material for the EM wave located in the PBG frequency range. The birefringence of bulk PhC is measured for the hexagonal lattice structure in microwave band and the experimental measurement birefringence is below 0.20 [8]. By increasing the index difference of the materials, the birefringence of the bulk PhC could be much stronger. Taking a bulk 2D structure as example, the PhC is composed by parallel cylinder dielectric rods in air, in which the dielectric rods have radius of r=0.37a and permittivity of ε=8.9 [26]. Choosing frequency range of 0.1-0.2 a/λ as the operating band which is below the first forbidden band (0.2495-0.2778 a/λ) of the TM polarization, the EM fields

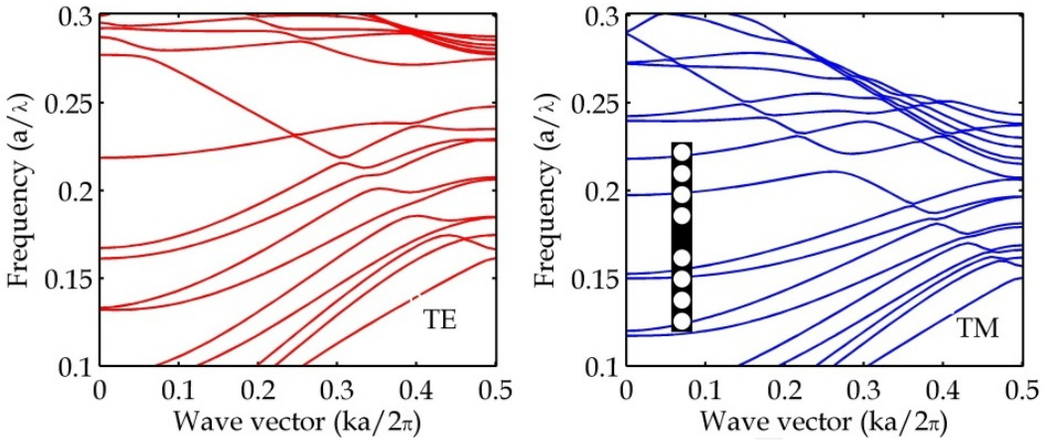


Figure 6. Dispersion curves of line defect square lattice PhCW. The inset is the 1×9*a* supercell used in PWE calculations. The parameters of the PhCW are chosen as follow: permittivity of high and low index materials are 12.96 and 1, respectively and the radius of air holes is *r*=0.40*a*.

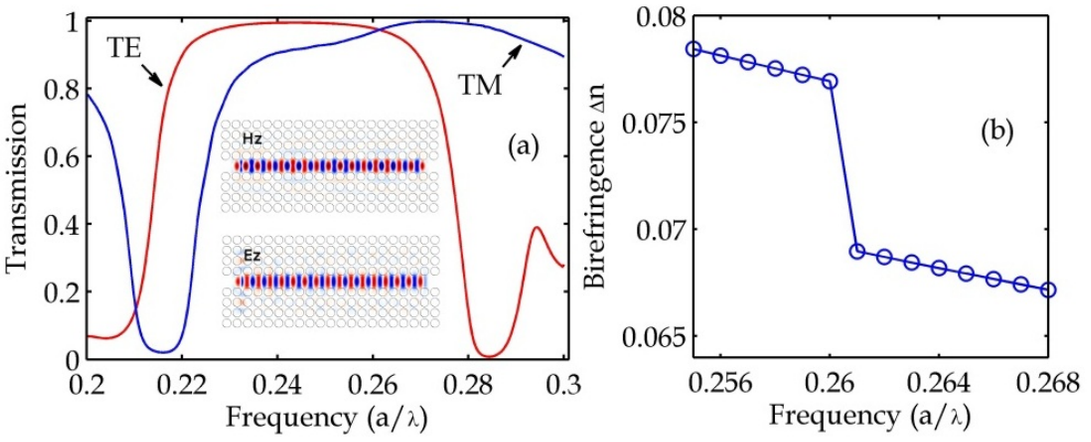


Figure 7. (a) Transmission spectra of the line defect square lattice PhCW. The insets are the EM field distributions for TE (H_z) and TM (E_z) polarization, respectively, at the frequency of 0.263 *a*/λ. (b) Birefringence (Δ*n*) of the PhCW calculated by SFT method. Structure used in FDTD and SFT simulation and the parameters of PhCW are as same as that in Fig. 6

propagate in the bulk PhC are shown in Fig. 8 (a). By using the SFT method, the birefringence of the studied bulk PhC are calculated and shown in Fig. 8 (b). The largest birefringence of the bulk PhC is about 0.8, which is much larger than that of the PhCW for the transmission path is almost homogeneous in the line defect of the PhCW but periodic in the bulk PhC.

For the birefringence related applications, the bulk PhC is a good candidate for the large birefringence in it, however, there are still some disadvantages [27]: 1) Lacking of effective light confining in the propagating plane makes beam divergence, as shown in Fig. 8 (a), which will spread the EM fields into the adjacent devices and cause crosstalk if there are many components packaged compactly, such as in PIC, to fulfill complicated functions. 2) The attenuation of light in the bulk PhC is high for the high scattering loss in it. These two problems should be solved in the practical applications such as WPs.

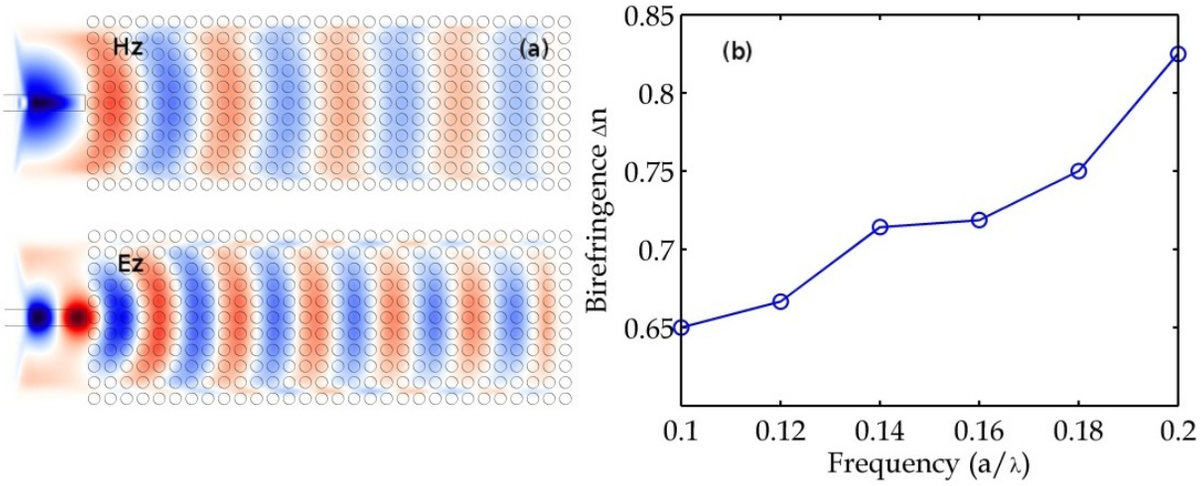


Figure 8. (a) EM fields propagate in the bulk PhC for TE (H_z) and TM (E_z) polarization, respectively, at the frequency of 0.10 a/λ. The CW source is excited in the conventional planar waveguide adjacent to the bulk PhC. (b) Birefringence (Δn) of the PhC calculated by SFT method. The calculated structure is a 2D bulk PhC with square lattice dielectric rods in air and the permittivity and the radius of dielectric rods are ε=8.9 and r=0.37a, respectively.

3.3. Birefringence of 1D PhCW

As shown in Fig. 9 (a), the 1D PhCW here refers in particular to the PDW [28-30], also known as nanopillar periodic waveguide [31-35] or coupled periodic waveguide [36], which has periodicity only in the light propagating direction. The 1D PhCW has attracted a lot of research interests for the simpler structure comparing with the 2D PhCW, and can be used in slow light [37], laser [35], low-loss waveguide [28-30, 38, 39], micro-resonator cavities [40], splitters for polarization and frequency [41-44], etc. The dispersion curves of the 1D PhCW could be examined by PWE method as what shown in Fig. 9 (b). There are guided modes under the light line and only single TE and TM modes are supported by the structure when the frequency is under 0.2065 a/λ. In the single mode frequency region, the TE and TM guided modes at the same frequency have different propagation constants which reveal the 1D PhCW is a birefringent media [12].

The birefringence properties of the 1D PhCW with cylinder dielectric rods in air are shown in Fig. 10, and all birefringence values are calculated in the single mode frequency band. The 1D PhCW has giant birefringence, which is larger than 1.5, when the permittivity of dielectric rods is 12.96. The higher the permittivity of dielectric rods is, the larger the birefringence is. The birefringence varies rapidly in the frequency band nearby the upper edge (slow light region) of the first TM guided mode when the 1D PhCW having relatively small dielectric rods (e.g. r=0.45a and r=0.50a). The largest birefringence appears at the edge of the slow light band. For the frequency outside the slow light band, the largest values of birefringence are almost equal for the 1D PhCW with different size of dielectric rods if the values of permittivity are same. There are *flat* sections in which the birefringence varies slowly ($d\Delta n/d\omega$~0) for the radius of 1D PhCW is be equal or greater than 0.50a, especially for r=0.50a as shown in the zoom-in curves in Fig. 10 (d). This reveals that the 1D PhCW has broadband achromatic birefringence. For example, the birefringence is between 1.1505 and 1.1530 in the frequency band of 0.167-0.188a/

http://dx.doi.org/10.5772/55142

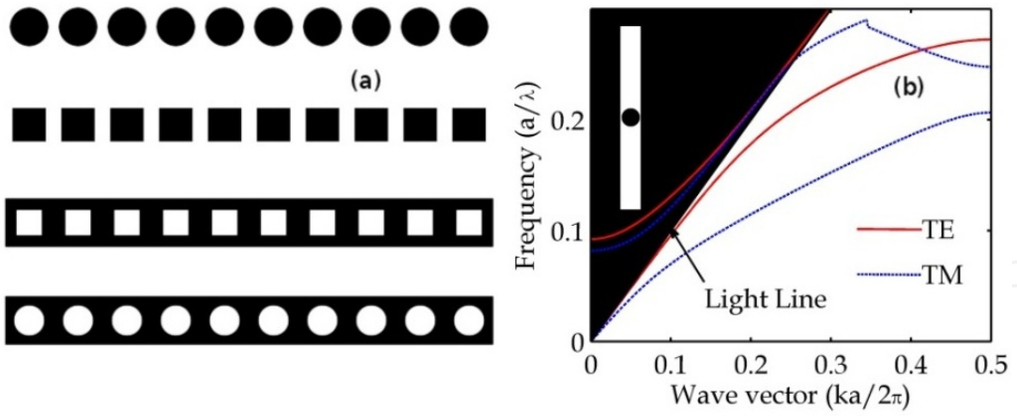


Figure 9. (a) Top view of the structures of different type of 1D PhCWs: cylinder and square dielectric rods in air, and square and cylinder air holes in dielectric waveguide, respectively, from top to bottom. (b) Dispersion curves of 1D PhCW with dielectric rods in air for both TE and TM polarizations. The inset is the 1×9*a* supercell used in PWE calculation, and the permittivity and the radius of dielectric rods are ε=8.9 and r=0.45*a*, respectively

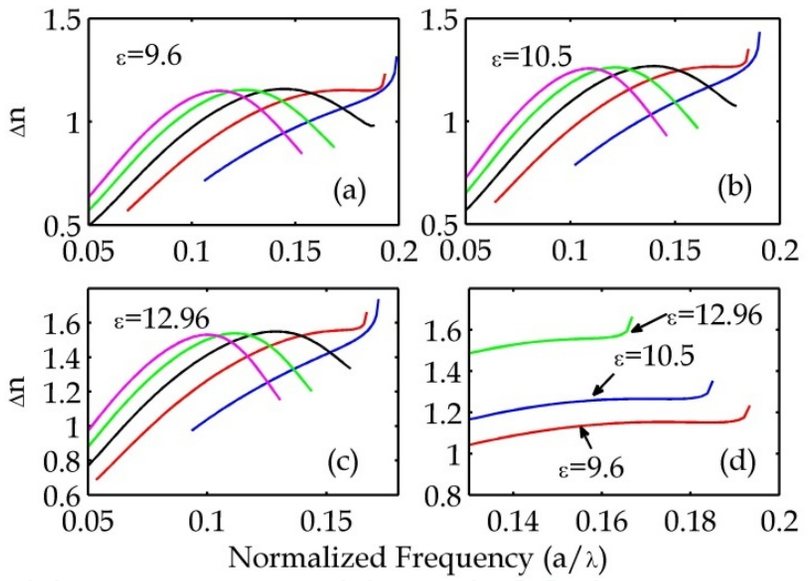


Figure 10. Birefringence of 1D PhCW with different parameters of (a) ε=9.6, (b) ε=10.5, and (c) ε=12.96, respectively. The blue, red, black, green and magenta lines represent the radius of dielectric rod equals 0.45*a*, 0.50*a*, 0.55*a*, 0.60*a*, and 0.65*a*, respectively. (d) Zoon-in picture of birefringence of 1D PhCW with radius of r=0.50*a*. [12]

λ when the dielectric rods have permittivity of ε=9.6, and for ε=10.5, the achromatic band is 0.165-0.178 a/λ in which the birefringence is 1.264-1.265 [12].

Other types of 1D PhCW have large birefringence too. Taking the 1D PhCW with square air holes in dielectric waveguide as example, the birefringence is around 1 when the length of side of the square is w=0.5*a*, and the permittivity and width of the dielectric waveguide are ε=12.96 and a, respectively [11]. Generally speaking, the 1D PhCW is better for birefringence related applications than the 2D PhCWs and bulk PhC for it has simple structure, low-loss and most important higher birefringence.

4. Ultracompact WPs based on PhC structures

One of the most important devices for birefringence related applications is WP which is worked as phase retarder. The phase difference ($\Delta\varphi$) between TE and TM polarization after propagating a distance of L can be expressed as $\Delta\varphi=2\pi\Delta nL/\lambda$, where Δn and λ are birefringence and wavelength, respectively. When the phase difference has relationship of $\Delta\varphi=m\pi/2$ and $\Delta\varphi=m\pi$, where m is an integer, the phase retarder is names as quarter-wave plate (QWP), and half-wave plate (HWP), respectively. Low-order (m is a small value) QWPs and HWPs have been investigated both theoretically and experimentally by different PhC structures. Although there are works to achieve $\pi/2$ and π phase retarding by reflecting EM wave at the stop band of perfect bulk PhC [45], most of the WPs are realized by the birefringence effect of the PhC structures. Compact transmissive QWPs and HWPs have been firstly analyzed theoretically by prof. Li [26] using bulk 2D PhC and soon after experimentally realized by Dr. Soli in microwave frequency [8, 46-49]. The WPs based on the birefringence effect of slab and bulk 2D PhCW are studied by numerical calculating in 2007 [9] and 2009 [10]. The ultracompact WPs with ultra-broadband achromatic phase difference are investigated by air-holes and dielectric rods 1D PhCW, recently [11, 12].

WPs with broadband achromatic phase difference are widely used in practice for the most of polarization-phase controlling devices require frequency independent phase retarding. Beyond that, compact in size is essential for that the original intention is realizing phase retarding in PICs for PhC structures based WPs. From the expression of the phase difference, the value of Δn is determinant of the size of WPs and the higher Δn is, the more compact the WP is, this gives the reason of the requirement of giant birefringence. It is a little complicated to achieve broadband achromatic phase difference for that $\Delta\varphi$ depends not only on Δn, but L, and λ as well. Slow-varying or constant maintaining of $\Delta\varphi$ relies on the envelope of $\Delta n/\lambda$, and the value of L. So, it is quite necessary for achromatic WPs that Δn should grows in a slow and linear fashion with wavelength in broadband. Meanwhile, choose L as small as possible, under the premise of that the requisite phase retarding could be realized, to avoid the enhancement of the non-uniformity of $\Delta n/\lambda$ at different wavelength. This is the cause of the low-order WPs are preferred in practical broadband applications. However, there are still some cases requiring $\Delta\varphi$ changing rapidly with frequency, i.e. high dispersion, in some particular applications such as polarization scrambling and depolarization. High-order WPs with large value of L is preferred to implement these functions. Except for operating band, dispersion, and size discussed above, the loss and compatibility should also be take into consideration in practically to evaluate the performance of WPs.

For the large and designable of birefringence in PhC structures, high performance WPs can be realized, such as low-order broad-band achromatic and high-order compact QWPs and HWPs. This section will focus on the low-order WPs based on 2D PhCW, 2D bulk PhC and 1D PhCW, respectively, and the compact high-order WPs based on the so called formed birefringence are discussed, too.

4.1. Low-order WPs based on 2D PhCW

For the simplicity of the 2D PhCW with hybrid PBG and TIR modes, the square lattice air holes type of PhCW studied in Fig. 6 and Fig. 7 is used to design the low-order WPs. The structure

http://dx.doi.org/10.5772/55142

used in the FDTD simulation is shown in Fig. 11 (a). A waveguide broadband Gaussian pulse source with width of a is excited at x=-6.5a, and point detectors located at different positions record the electric fields by which the phase shift (Φ) of TE and TM polarizations are obtained. Fig. 11 (b) and (c) give the phase shifts at x=13.1a and x=27.1a, respectively, on the initial phase which obtained at x=-0.5a where the phase differences ($\Delta\varphi$) between TE and TM modes are zero at the operating frequency band. The unwrapping $\Delta\varphi$ are shown in Fig. 11 (d) and (e), correspondingly. The values of $\Delta\varphi$ are about $\pi/2$ (QWP) and π (HWP) at x=13.1a and x=27.1a, respectively, with high phase accuracy of $\pm 0.005\pi$ in the frequency range of 0.2632-0.2642 a/λ for both QWP and HWP. The relative achromatic bandwidth is about 0.38%. The length of 2D PhCW that introduce $\pi/2$ phase difference between TE and TM polarization is about $L_{\pi/2}$=27.1a-13.1a =14a, which is in good agreement with that obtained by SFT method, e.g. the length is about 13.9a when ω=0.264 a/λ for the birefringence at this wavelength is about Δn= 0.0682 as shown in Fig. 7 (b). So, the length of the zero-order QWP and HWP is about 3.7λ and 7.4λ, respectively. Although not shown here, the phase characteristics can also be verified in separate frequency by launching CW source in the waveguide and recording the EM field variation in time. The size of WPs can be reduced, although not too much, by the triangular

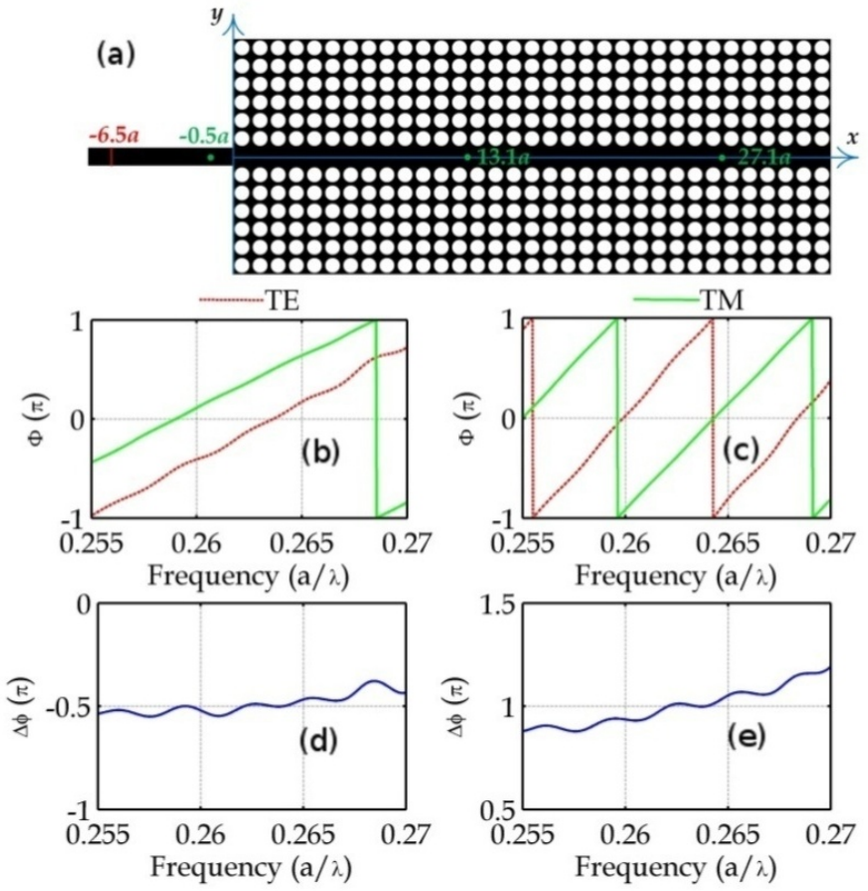


Figure 11. (a) Structure used in simulations. The parameters of the 2D PhCW are as same as that in Fig. 6 and Fig. 7. [(b), (c)] The phase (Φ) at (b) x= 13.1a and (c) x=27.1a, respectively. [(d), (e)] Unwrapping phase difference ($\Delta\varphi$) at (d) x= 13.1a and (e) x=27.1a, respectively. [10]

lattice 2D PhCW for the birefringence in it is larger than the square lattice one. However, it must be admitted that the PhCW has no advantages comparing with the other PhC structure in size and achromatic bandwidth, the only merit may be the guiding and confining of light is perfect in 2D PhCW.

4.2. Low-order WPs based on bulk 2D PhCs

The bulk 2D PhC has larger birefringence than the 2D PhCW, therefore, the WPs realized by bulk PhC has smaller size. However, the beam divergence is severe in the perfect PhC structure as discussed before and the divergent beam in nonwaveguiding structure will interfere with other components for large number of devices integrated in ultrasmall space in practical PICs [27]. Interference and scattering loss caused by beam divergence can be solved by the so called self-collimating (SC) effect under which light beam can propagate with no diffraction in perfect PhCs [50-52].

Polarization independent SC propagation is need in PhC for the WP applications. As shown in the inset of Fig.12 (a), the designed PhC is square lattice air holes in dielectric materials, and the permittivity of host material and radius of air holes are ε=11.0224 and r=0.315a, respectively [27]. The band structure is calculated by PWE method and shown in Fig. 12 (a). The equal frequency contours near the frequency band marked as green shallow region in Fig. 12 (a) are plotted in Fig. 12 (b) and (c) for TM and TE polarization, respectively. From the figures, both TE and TM have ultra-flat equifrequency surface in the frequency band of 0.273-0.281 a/λ. As

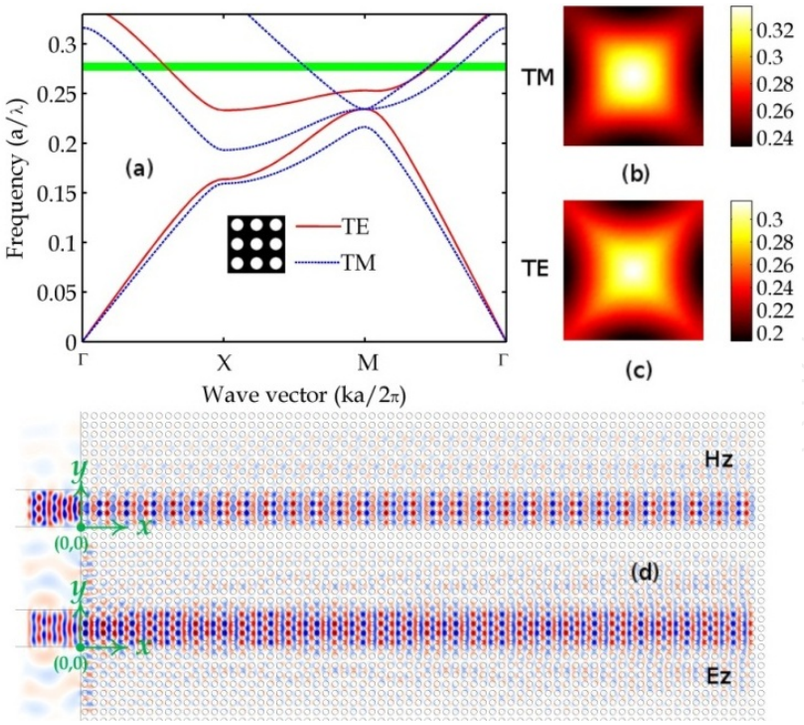


Figure 12. (a) Band structure of the square lattice PhC with polarization independent SC effect. [(b), (c)] Equal frequency contours for TM (b) and TE (c) polarizations. (d) Snapshots of the EM fields distributions at the frequency of 0.274 a/λ for TE (H_z) and TM (E_z) polarizations.

http://dx.doi.org/10.5772/55142

the direction of light propagation is always normal to the equifrequency surface, the light will propagate in the PhC without divergence along the <0 1> direction for both TE and TM polarizations, which can be seen clearly in Fig. 12 (d).

By launching broadband Gaussian pulse source in the coupling waveguide (refer Fig. 12 (d)), the transmission behaviors of the SC beam in the PhC are quantified and the spectra are shown in Fig. 13 (a) and (b) for TE and TM polarization, respectively. In the polarization independent SC band, the transmission efficiencies are above 75% for both TE and TM polarizations when the length is shorter than 70*a*. This is a significant improvement over the conventional PhC without SC guiding effect. Same as what have done in the section 4.1, the phase shift for TE and TM polarizations are calculated by using the recorded EM fields. Fig. 13 (c) and (d) show the phase shifts (Φ) and unwrapping phase difference ($\Delta\varphi$) at positions of 10*a* and 12*a*, respectively. During the simulation, the initial phases are obtained at −4*a*. In a wide band region of 0.273-0.281 a/λ, the values of $\Delta\varphi$ are almost constants of $\pi/2$ (QWP) and π (HWP) when the lengths of the PhC are 10*a* and 12*a*, respectively. For both QWP and HWP, the phase accuracy is about $\pm 0.01\pi$, and the transmission efficiencies are above 96%. The relative spectral bandwidth of the designed WP is about 3%, which is about the half of that of dense wavelength division multiplexing (DWDM) optical communication systems. Although the bandwidth of the WPs is not wide enough to cover all the frequency range of DWDM systems, it is as wide as 45 nm and is wide enough for many applications. The fact that should be indicated is that the 10*a* and 12*a* length WPs are not the zero-order ones. The lower-order WPs may have broader achromatic frequency band.

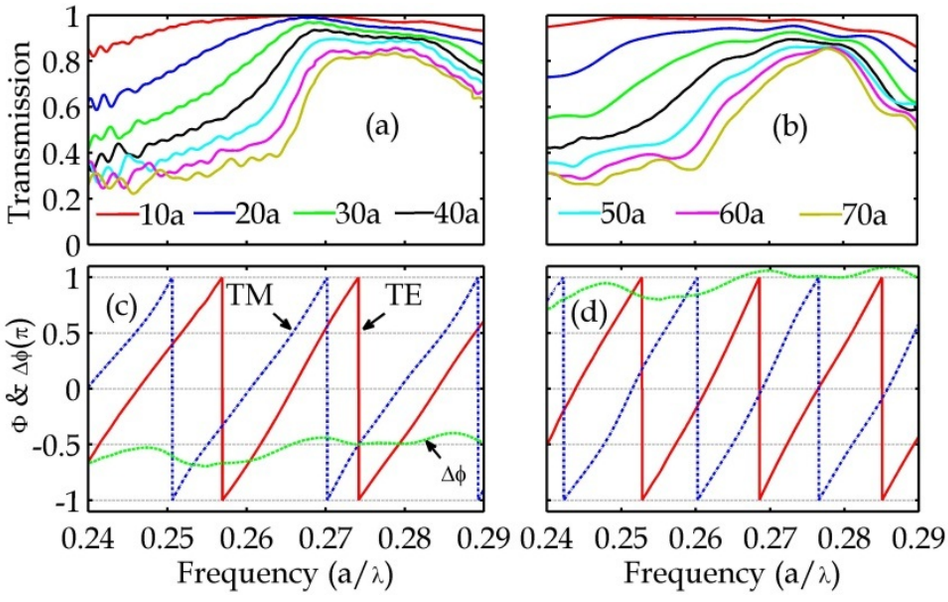


Figure 13. [(a), (b)] Transmission spectra for TE (a) and TM (b) polarizations. [c, d] Phase (Φ) and phase difference ($\Delta\varphi$) at x=10*a* and x=12*a*, respectively. [27]

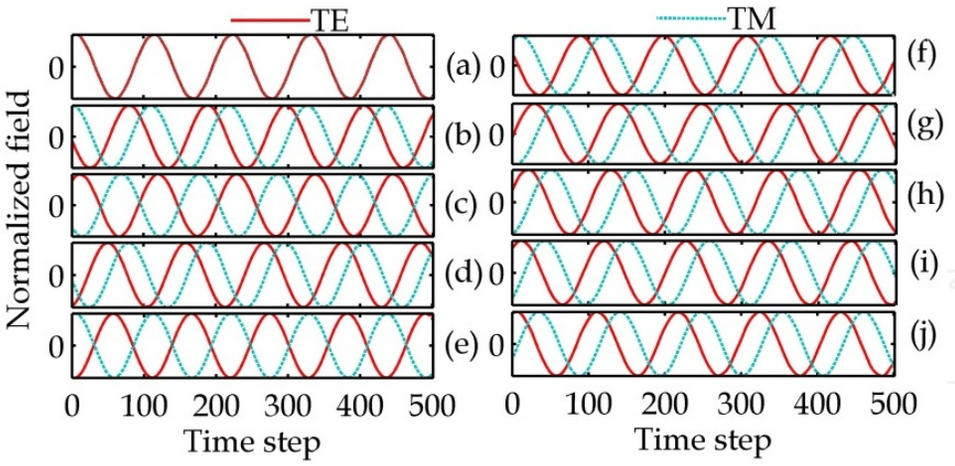


Figure 14. Normalized EM fields variations with time for TE and TM polarizations at different space locations and EM wave frequencies. [(a)-(e)] With the same frequency of 0.275 a/λ and at different positions of x=-4a (a), 10a (b), 12a (c), 50.4a (d) and 50.7a (e), respectively. [(f)-(j)]. At the same location of x=10a, but with different frequency of ω=0.273 a/λ (f), 0.274 a/λ (g), 0.276 a/λ (h), 0.278 a/λ (i), and 0.280 a/λ (j), respectively. [27]

To verify the phase characteristics of the WPs designed above, a CW source is launched in the dielectric waveguide, and a set of point monitors are inserted along the x direction in the center of the light beam in y direction to detect the electric fields (E_y for TE and E_z for TM) at different times. The phases of TE and TM at the reference position x=−4a are identical at the frequency 0.275 a/λ [see Fig. 14 (a)], which reveals zero phase difference between TE and TM polarizations. After propagating to 10a, as shown in Fig. 14 (b), the phase difference between TE and TM is about $\pi/2$. Furthermore, at 12a, TE and TM reverse in phase [see Fig. 14 (c)]. These results certify that the WPs work effectively at the frequency 0.275 a/λ. Higher-order QWP and HWP also can be realized (as shown in Fig. 14 (d) and (e)) for the light can propagate a relatively long way in PhC with the help of SC effect. To verify the broadband characteristic of the WPs, one monitor is set at 10a, and the frequency of source is changed. Fig. 14 (f)–(j) show that the 10a length QWPs have an almost fixed phase difference of $\pi/2$ (accuracy of $\pm 0.01\pi$) in a wide frequency range. Although not shown in the figures, similar broadband characteristics have been obtained for 12a length HWPs with the same simulation method.

4.3. Low-order WPs based on 1D PhCW

Comparing with the 2D PhCW, 1D PhCW has larger birefringence, so that it is very suitable for the ultracompact low-order WP applications. Both 1D PhCW with dielectric rods in air and air holes in dielectric waveguides have been used to design high performance WPs.

4.3.1. Low-order WPs based on 1D PhCW with dielectric rods in air

The birefringence properties of 1D PhCW with dielectric rods in air have been studied thoroughly in section 3.3. Although there is broadband achromatic birefringence, it is not enough to achieve wide band achromatic phase difference for $\Delta\varphi$ is also determined by L and λ. Actually, the structure supporting achromatic $\Delta\varphi$ is $r \geq 0.55a$ which is different from the critical value of 0.50a for achromatic birefringence.

http://dx.doi.org/10.5772/55142

For the ultrahigh birefringence, 2π phase difference ($\Delta\varphi=2\pi$) can be introduced by 1D PhCW with short length even smaller than the operating wavelength λ if Δn is large enough. Taking the 1D PhCW with ε=12.96 and r=0.55a as an example, if the operating frequency is ω=0.145 a/λ, 2π phase difference is introduced by the structure with length of L=4.63a, which is smaller than the wavelength of λ=6.9a, for the birefringence at the frequency is Δn=1.488 from Fig. 10. By using the FDTD simulation scheme, the characteristics of this 1D PhCW based WPs are verified. The normalized EM fields for TE (E_y) and TM (E_z) polarizations are shown in Fig. 15 (a)-(j). The phases of TE and TM are identical at location of x=3.4a as shown in Fig. 15 (a). After propagating to 4.5a, as shown in Fig. 15(b), the phase difference between TE and TM is $\pi/2$. Furthermore, the phase differences are π [see Fig. 15(c)], $3\pi/2$ [see Fig. 5(d)], and 2π [see Fig. 5(e)] at the positions of 5.55a, 6.55a, and 8.0a, respectively. These results certify that the 1D PhCW with length of 4.5a and 5.55a (the real lengths are about 0.6525λ and 0.80475λ, respectively) can be served as the first-order QWP and HWP at frequency of 0.145 a/λ, respectively. The phase difference of 2π is introduced by the length of $L_{2\pi}$=8.0a-3.4a=4.6a, and this is in good agreement with the theoretical value of 4.63a calculated above. To verify the broadband achromatic properties of the phase difference, CW sources with different frequencies are launched into the PDW, and the detector is located at x=4.5a unchanged. Fig. 15(f)–(j) show that the phase differences are fixed at $\pi/2$ in frequency range of 0.140–0.150a/λ. The relative bandwidth is about 28% which is much wider than that of the 2D PhCW and bulk PhC. If taking the central frequency 0.145 a/λ as λ=1550 nm (a=224.8 nm), the real frequency bands are from 1498nm to 1605 nm, which almost covers the whole telecommunication band containing C, L and S. [12].

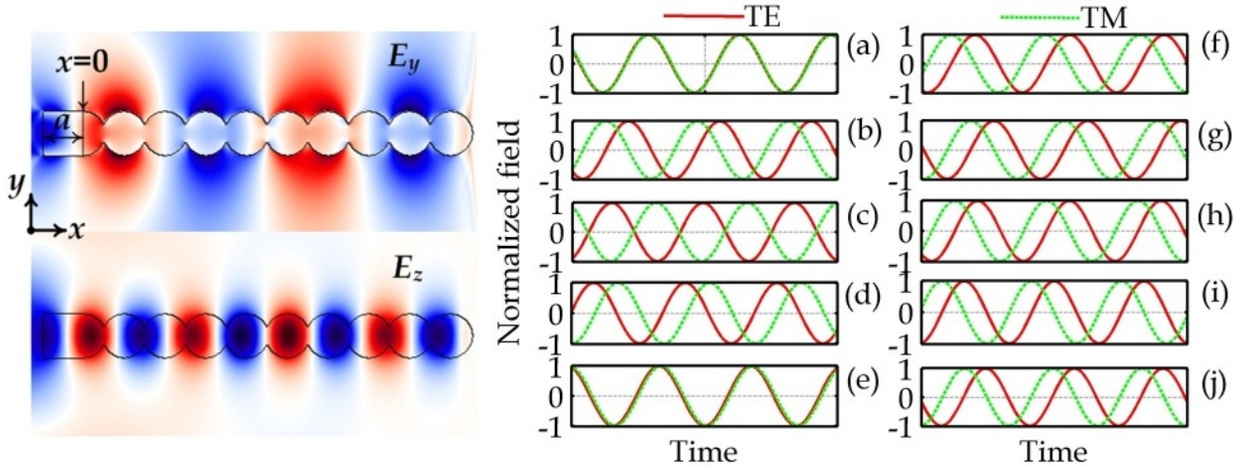


Figure 15. [Left] Snapshots of the EM fields for TE (E_y) and TM (E_z) polarizations. The simulation structure is shown in the figure as background. [Right] Normalized EM fields variations with time for TE and TM polarizations at different space locations and EM wave frequencies. The left column is ω=0.145 a/λ at different locations of 3.4a (a), 4.5a (b), 5.55a (c), 6.55a (d), and 8.0a (e), respectively. The right column is x=4.5a with different frequency of 0.140 a/λ (f), 0.142 a/λ (g), 0.145 a/λ (h), 0.148 a/λ (i), and 0.150 a/λ (j), respectively. [12]

Except for the waveguide dispersion, the material dispersion also can affect the effective indices of the waveguide modes, and then affect the birefringence. To study the phase difference of 1D PhCW with dispersive material, Silicon (Si) is chosen as the material of dielectric rods for the permittivity of Si can be obtained by Sellmeier formula:

$$\varepsilon = 11.6858 + \frac{0.939816}{\lambda^2} + \frac{0.000993358}{\lambda^2 - 1.22567} \tag{4}$$

where the wavelength λ is in μm. The radius of the Si rods is 0.55a. The phase difference ($\Delta\varphi$) of Si 1D PhCW with length of L=4a and L=6a are shown in Fig. 16. Although the material dispersion affects the birefringence of 1D PhCW, there is broadband achromatic phase difference for the Si 1D PhCW. The achromatic bandwidth is larger than 100nm with excellent phase accuracy of ±1°. The achromatic band can be tuned by changing the lattice constant a, and it is red shift by increasing the value of a. The bandwidth is affected by the length of 1D PhCW. Taking a=240nm as example, with the same accuracy of ±1°, the bandwidth is about 125nm (1495-1620nm, 301±1°) when L=4a, and about 100nm (1506-1606nm, 452±1°) when L=6a. Just as discussed before, the achromatic band is narrower when the length of 1D PhCW is longer. For the Si 1D PhCW, the material dispersion does affect the phase difference of TE and TM modes propagate in it, but does not restrict the realization of broadband achromatic WPs.

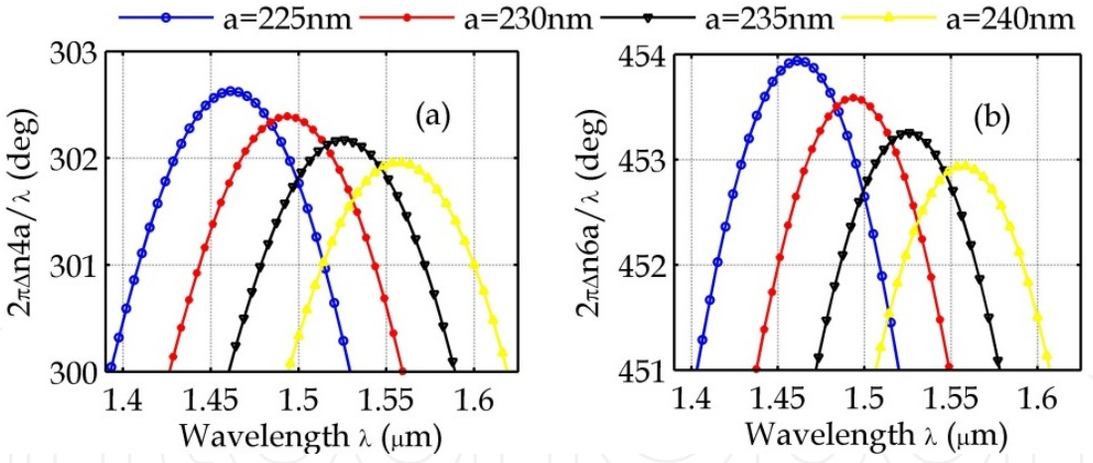


Figure 16. Phase difference of Si 1D PhCW with L=4a (a) and L=6a (b), respectively. The radius of Si rods is r=0.55a, and the indices of Si are calculated by Eq. (4). [12]

4.3.2. Low-order WPs based on 1D PhCW with air holes in dielectric waveguide

Another type of 1D PhCW is the periodic air holes in dielectric waveguide as shown in Fig. 9 (c) and (d). This type of structure is easier integrated with other components for the most of devices in PIC are constructed and interconnected by waveguide. Here, the 1D PhCW with square air holes is used to design high performance low-order WPs. The width of the waveguide is as same as lattice constant a, the length of square's side is w=0.5a, and the permittivity

of the high index material is 13. Although not shown, the birefringence of this 1D PhCW is larger than 1 in the single mode frequency range of 0.1-0.15 a/λ.

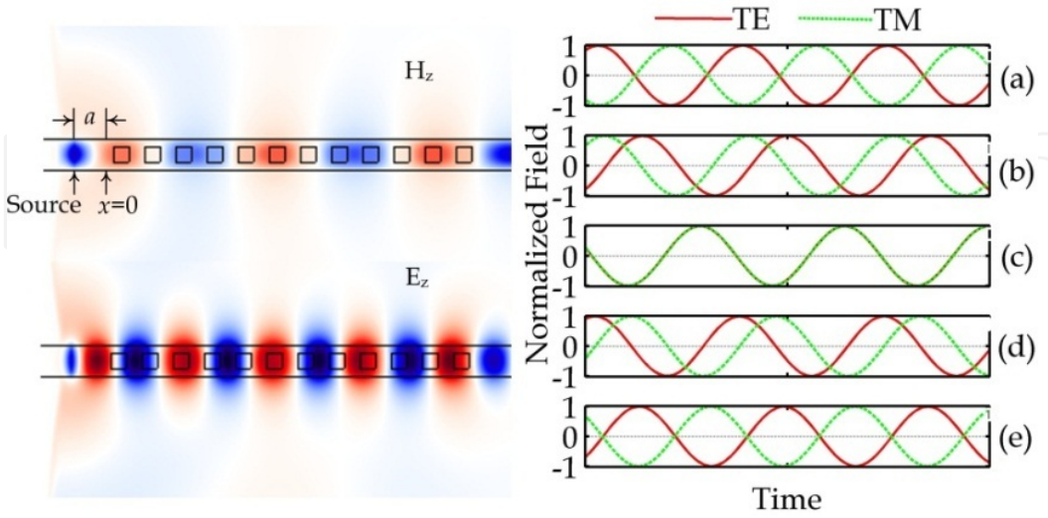


Figure 17. [Left] Snapshots of EM fields at frequency of 0.14 a/λ for TE (H_z) and TM (E_z) polarizations.[Right] Normalized EM field variations with time for TE and TM modes with same frequency of 0.14 a/λ but at different space locations of 2.9a (a), 4.45a (b), 6.4a (c), 7.9a (d), and 89.6a (e), respectively. [11]

The phase differences between TE and TM polarizations are directly studied by FDTD simulation method. A CW source with frequency of ω=0.14 a/λ is excited in the waveguide at position of x=-a, and several point monitors are placed at different positions along x direction at the center of the propagation beam in y direction. The snapshots of the EM fields in the 1D PhCW are shown in Fig. 17 (left) and the recorded electric fields at different positions are shown in Fig. 17 (a)-(e). From the figures, the phase differences ($\Delta\varphi$) at x=2.9a, x=4.45a, x=6.4a, x=7.9a, and x=9.6a are π, 3π/2, 2π, 5π/2, and 3π, respectively. As a result, the structures with length, which contains length of adjacent coupling waveguide and 1D PhCW, of 3.9a, 5.45a, 8.9a, and 10.6a can serve as HWP, QWP, QWP, and HWP, correspond real length of 0.546λ, 0.763λ, 1.246λ, and 1.484λ, respectively. The phase difference of 2π is introduced by the distance of 6.7a and this is in good agreement with the value of 6.5a calculated by PWE method.

The shortage of the structure studied above, referring to nontaper structure, is that the transmission loss is relatively high as shown in Fig. 18 (a) and (b).To reduce the loss, a taper structure is used to design high performance WP and the structure is shown at the top of Fig. 18.The transmission efficiencies are effectively improved by the taper 1D PhCW with w_1=0.35a, and w_2=0.5a, especially for TM polarization. The transmission efficiency is more than 90% in the frequency range of 0.139-0.148 a/λ for both TE and TM polarizations. The efficiency can be improved further by optimizing the taper structure. The phase differences are around π/2 for different frequencies from 0.139 a/λ to 0.148 a/λ as shown in Fig. 18 (c)-(f). The taper with total length of 5a can serve as broadband QWP, although the phase accuracy is not very high (±0.02π). The phase accuracy also can be improved by carefully tuning the parameters of the taper.

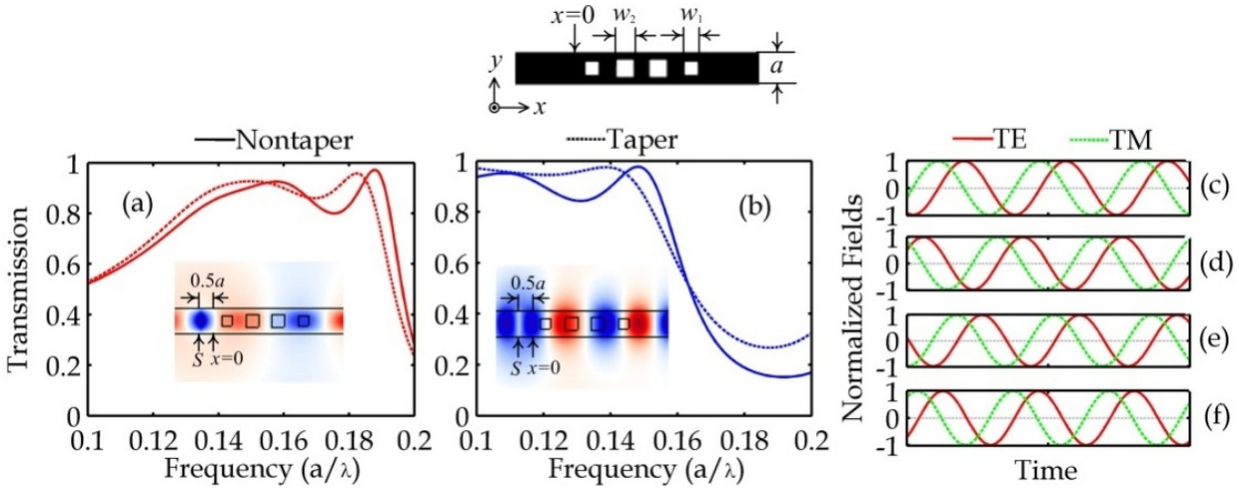


Figure 18. [a-b] Transmission spectra for square air hole 1D PhCW with conventional structure and taper structure for both TE (a) and TM (b) polarizations. The insets in (a) and (b) are snapshots of the EM fields propagating in the taper structure at frequency of 0.14 *a*/λ for TE and TM polarizations, respectively. The structure of the taper is shown at the top and the wave source is excited at *x*=-0.5*a*.[c-f] Normalized electric fields of E_y (TE) and E_z (TM) in the taper structure at positions of *x*=4*a* with frequency of 0.139 *a*/λ (c), 0.142 *a*/λ (d), 0.145 *a*/λ (e), and 0.148 *a*/λ (f), respectively. [11]

4.4. High-order WPs based on formed birefringence effect

Except for the low-order achromatic WPs, high-order WPs are also useful in some special applications. By increasing the length of the PhC structures, high-order WPs can be realized, but it is not inadvisable when the birefringence is not large enough and the loss increases rapidly with the increasing of length. Another method to realize high-order WPs proposed before is so-called formed birefringence which takes full advantage of birefringence and optical path difference between TE and TM polarizations [27, 10, 12].The schematic diagram is shown in Fig. 19 (a). The key point of the formed birefringence is bringing path difference of two orthogonal polarizations into use to enhance the phase difference between them. As that shown in Fig. 19 (a), the lengths of path for polarization 1 (TE or TM) and polarization 2 (TM or TE) are denoted as L_1 and L_2, respectively. The effective indices are n_1 and n_2, correspondingly, and supposing that $n_2 > n_1$. The total phase difference between two polarizations after propagating through two paths can be expressed as:

$$\Delta\varphi_{\text{tol}} = \frac{2\pi}{\lambda}\left(n_2 L_2 - n_1 L_1\right) + \varphi_0 \tag{5}$$

where φ_0 is the total phase difference caused by other factor such as reflection in the interfaces. Eq. (5) can be further written as

http://dx.doi.org/10.5772/55142

$$\Delta\varphi_{\text{tol}} = \frac{2\pi}{\lambda}\Delta n L_1 + \frac{2\pi}{\lambda} n_2 \Delta L + \varphi_0 \tag{6}$$

where $\Delta n = n_2 - n_1$ is the birefringence and $\Delta L = L_2 - L_1$ is the length difference of paths. The three items of the phase difference in Eq. (6) are caused by birefringence, path difference and other factors, respectively. In most case, the effective index is larger than the birefringence ($n_2 > \Delta n$), so, the total phase difference will be enormously enhance if using the path difference effectively.

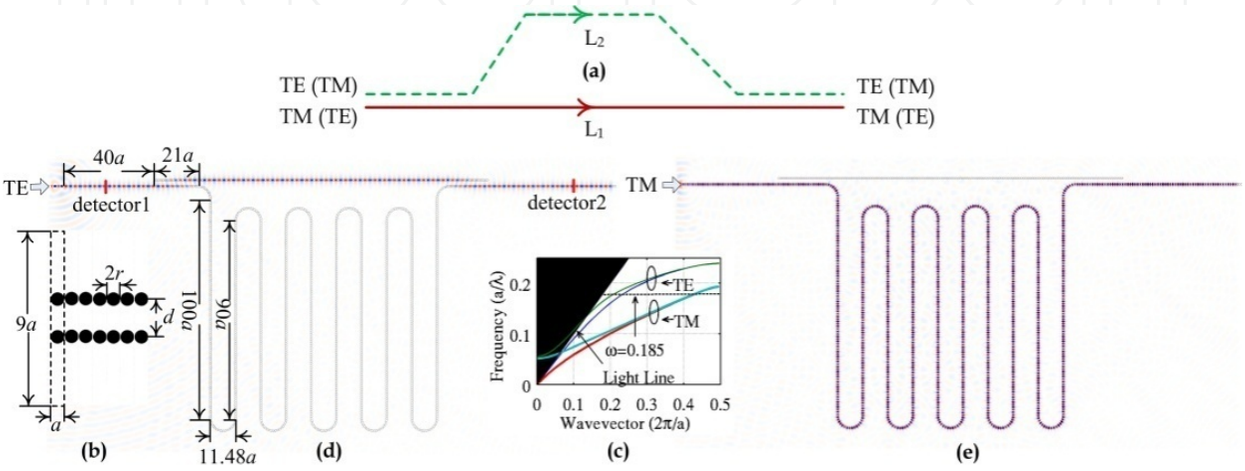


Figure 19. (a) The schematic diagram of formed birefringence (b) Structure of the direct coupler used as PBS and PBC and the supercell used in PWE calculations. (c) Band structure of the direct coupler. [(d),(e)] Snapshots of the EM fields at frequency of 0.185 a/λ for (d) TE (H_z) and (e) TM (E_z) polarizations. [12]

The high-order WP by formed birefringence effect is designed based on dielectric rod type of 1D PhCW with ε=9.6 and r=0.5a. The structure is composed by two coupling waveguides, which serve as input and output ports, and two direct couplers, which are used for polarization beam splitting and combining. As shown in Fig. 19 (b), the direct coupler is constituted by two parallel 1D PhCW placed closely with distance of d=2.8a. The dispersion curves of the two parallel rows of dilectric rods are calculated by PWE method with 1×9a supercell (shown in Fig. 19 (b)) and are shown in Fig. 19 (c). From the figure, the first and second TM modes are superposed but two lowest TE modes are separate with each other at the frequency of 0.185 a/λ. According to the direction coupling length equation, $L_c = \pi/\Delta k$, the coupling length is an infinitely large number for TM polarization for the wave vector difference (Δk) of first and second modes are zero. For the TE modes, the first and second modes can coupled to each other completely after propagating a length of L_c which is determined by Δk. The length of the direct coupler is optimized to L_c=21a to couple the mode from one waveguide to another in broadband. From the dispersion curve of the 1D PhCW, the effective index of TM mode (n_{TM}) is larger than that of the TE mode (n_{TE}), so, the propagation route of the TM mode is chosen as a zigzag path to make the TM mode having larger propagating length, which is shown in the background of Fig. 19 (d) and (e). To reduce the loss of the bend, the bend diameter is chosen as a relatively large value of 11.48a. The other parameters of the whole structure of designed

high-order WP can also be found in Fig. 19. The whole size of the simulation is about 240×120a.The snapshots of the EM fields at the frequency of 0.185 a/λ for TE (H_z) and TM (E_z) polarization are shown in Fig. 19 (d) and (e), respectively. According to Eq. (6) and by using the parameters of Δn=1.1505, L_1=240a, ΔL=980a, n_2=n_{TM} =2.4427, and ω=0.185 a/λ, the phase difference caused by birefringence and formed birefringence are about 102π and 886π, respectively. Neglecting φ_0 (generally, it is a small value), the total phase difference is about $\Delta\varphi_{tol}$=1000π, and it can serve as a 500th-order WP. It can depolarize a laser with full width at half maximum that is wider than 3.1 nm [53] and can be used in the depolarization of a Raman pump laser diode and super-luminescence LED used in the fiber gyro. Taking λ=1550nm as an example, the lattice constant a is about 287nm. Therefore, the whole size of the 500th-order WP based on formed birefringence is about 69×34.5 μm.

Except for the 1D PhCW, the bulk PhC with polarization independent SC effect and the 2D PhCW are also can be used to design high-order WPs based on formed birefringence effect. The polarization beam splitter and combiner can be realized by direct coupler in 2D PhCW structure, and by reflecting and transmitting mirror in bulk PhC structure. Actually, the 80th order WP has been designed by the 2D PhCW with triangular lattice air holes in high index dielectric material [10].

5. Conclusion

In this chapter, the birefringence properties of three types of PhC structures, containing 2D PhCW, 2D bulk PhC, and 1D PhCW, have been studied thoroughly. High performance WPs based on the birefringence of these three types of PhC structures have been proposed. The comprehensive remarks about the three PhC structures are shown in Table 2.

For the 2D PhCW, the birefringence is not very high, so that the size of the WPs based on it is in wavelength magnitude. Although the achromatic bandwidth is not very large, 2D the PhCW provide perfect guiding for the light in it.

For the 2D bulk PhC, the birefringence in it is much larger than that in 2D PhCW. The disadvantage of the bulk PhC is the beam divergence which will cause scattering loss and signal crosstalk. This problem has been improved by the SC effect in this chapter. The WPs based on the 2D PhC with polarization independent SC effect have compact size and broad achromatic bandwidth (about 45nm).

For the 1D PhCW, giant birefringence, which is even larger than 1.5, can be realized in special structures. The 1D PhCW is very suitable for WP applications for its giant birefringence, low loss and compact in size. The achromatic bandwidth of the WPs based on 1D PhCW can be larger than 100nm with excellent phase accuracy of ±1°. Meanwhile, the size of the WP is in sub-wavelength magnitude.

Besides, the high-order WPs based on so called formed birefringence is proposed too. Additional phase differences are introduced by the path difference of different polarizations. The 500th order WP is designed based on the formed birefringence by using the 1D PhCW.

	Birefringence	Achromatic phase bandwidth	High orders	Length ($\Delta\varphi=2\pi$)	Loss
2D PhCW	~0.1	~6nm (±0.005π)	80	3.7λ	Low
Bulk PhC	~0.8	~45nm (±0.01π)	-	-	Relatively high
1D PhCW	~1.5	"/>100nm (±1°)	500	0.67λ	Low

Table 2. Comparing of the properties of three types of PhC structures

The WP is one of the basic elements in optical devices. The proposed PhC structure based WPs have a lot potential applications in future PICs for sensing, optical communications and measurements.

Acknowledgements

The authors would like to gratefully acknowledge W. –P. Huang at McMaster University, J. –W. Mu at MIT and J. Liu at Xi'an University of Posts and Telecommunications for their fruitful suggestion. The study was supported by CAS/SAFEA International Partnership Program for Creative Research Teams, West Light Foundation of The Chinese Academy of Sciences, and National Natural Science Foundation of China (Grant No. 61275062).

Author details

Wenfu Zhang and Wei Zhao

State Key Laboratory of Transient Optics and Photonics, Xi'an Institute of Optics and Precision Mechanics, Chinese Academy of Sciences, Xi'an, China

References

[1] Hsu, S., Lee, K., Lin, E., Lee, M., & Wei, P. Giant birefringence induced by plasmonic-nanoslit arrays, *Appl. Phys. Lett.*, 95: 013105 (2009).

[2] Weber, M. F., Stover,C. A., Gilbert, L. R., Nevitt, T. J., & Ouderkirk,A. J. Giant birefringent optics in multilayer polymermirrors, *Science*, 287: 2451 (2000).

[3] Muskens,O. L.,Borgström, M. T., Bakkers, E. P. A. M., & Gómez Rivas, J. Giant optical birefringence in ensembles of semiconductor nanowires, *Appl. Phys. Lett.*, 89: 233117 (2006).

[4] Weis, P., Paul, O., Imhof, C., Beigang, R., & Rahm, M. Strongly birefringent metamaterials as negative index terahertz wave plates, *Appl. Phys. Lett.*, 95: 171104 (2009).

[5] Yang, S., Cooper, M. L., Bandaru, P. R., & Mookherjea, S. Giant birefringence in multi-slotted silicon nanophotonic waveguides, *Opt. Express*, 16: 8306 (2008).

[6] Genereux, F., Leonard, S. W., & Van Driel,H. M. Large birefringence in two-dimensional silicon photonic crystals, *Phys. Rev. B, Condens. Matter,* 63: 161101 (2000).

[7] Xiao, X., Hou, B., Wen, W., & Sheng, P. Tuning birefringence by using two-dimensional photonic band structure, *J. Appl. Phys.*, 106: 086103 (2009).

[8] Solli, D. R., McCormich, C. F., Chiao, R. Y., & Hickmann, J. M. Birefringence in two-dimensional bulk photonic crystals applied to the construction of quarter waveplates, *Opt. Express* 11: 125 (2003).

[9] Bayat, K., Chaudhuri, S. K., & Safavi-Naeini, S. Design and simulation of an ultracompact integrated wave plate using photonic crystal slab waveguide, *Proc. SPIE* 6468: 64680N (2007).

[10] Zhang, W., Liu, J., Huang, W.-P., & Zhao, W. Birefringence and formed birefringence in photonic crystal line waveguides, *Proc. SPIE* 7516: 751603 (2009).

[11] Zhang, W., Liu, J., Huang, W. –P., & Zhao, W. Ultracompact wave plates by air holes periodic dielectric waveguides, *Proc. SPIE* 7609: 76091H (2010).

[12] Zhang, W., Liu, J., Huang, W. –P., & Zhao, W. Giant birefringence of periodic dielectric waveguides, *IEEE Photon. J.*, 3: 512 (2011).

[13] Yablonovitch, E. Inhibited spontaneous emission in solid-state physics and electronics, *Phys. Rev. Lett.*, 58: 2059 (1987).

[14] John, S. Strong localization of photons in certain disordered dielectric superlattices, *Phys. Rev. Lett.*, 58:2486 (1987).

[15] Joannnopoulos, J. D., Johnson, S. G., Winn, J. N. & Meade, R. D. *Photonic Crystals: Molding the Flow of Light,Second Edition*, Princeton University Press, 2008.

[16] Johnson, S. G. & Joannopoulos, J. D. Block-iterative frequency-domain methods for Maxwell's equations in aplanewave basis, *Opt. Express,* 8: 173 (2001).

[17] Taflove, A. & Hagness, S.C. *Computational Electrodynamics: The Finite-Difference Time-Domain Method*, Artech House Publishers, 2005.

[18] Oskooi, A. F., Roundy, D., Ibanescu, M., Bermel, P., Joannopoulos, J. D., & Johnson, S. G. MEEP: A flexible free-software package for electromagnetic simulations by the FDTD method, *Comput. Phys. Commun.*, 181: 687 (2010).

[19] Yee, K. Numerical solution of initial boundary value problems involving Maxwell's equations in isotropic media, *IEEE Transactions on Antennas and Propagation*, 14: 302. (1966).

[20] Jafarpour, A., Reinke, C. M., Adibi, A., Xu, Y., & Lee, R. K. A new method for the calculation of the dispersion of nonperiodic photonic crystal waveguides, *IEEE J. Quantum Electron.,* 40: 1060 (2004).

[21] Adibi, A., Xu, Y., Lee, R. K., Yariv, A.& Scherer, A. Guiding mechanisms in dielectric-core photonic-crystal waveguides, *Phys. Rev. B*, 63: 033308 (2001).

[22] Borel, P. I., Frandsen, L. H., Thorhauge, M., Harpoth, A., Zhuang,Y. X., Kristensen, M., & Chong, H. M. H. Efficient propagation of TM polarized light in photonic crystal components exhibiting band gaps forTE polarized light, *Opt. Express,*11: 1757 (2003).

[23] Zhang, W., Liu, J., & Zhao, W. Design of a compact photonic-crystal-based polarization channel drop filter, *IEEE Photon. Technol. Lett.*, 21: 739 (2009).

[24] Tsuji, Y., Morita, Y., & Hirayama, K. Photonic crystal waveguidebased on 2-D photonic crystal with absolute photonic band gap, *IEEEPhoton. Technol. Lett.*, 18: 2410 (2006).

[25] Morita, Y., Tsuji, Y., & Hirayama, K. Proposal for a compactresonant-coupling-type polarization splitter based on photonic crystalwaveguide with absolute photonic bandgap, *IEEE Photon. Technol.Lett.*, 20: 93 (2008).

[26] Li, L.-M. Two-dimensional photonic crystals: candidatefor wave plates, *Appl. Phys. Lett.*, 78: 3400 (2001).

[27] Zhang, W., Liu, J., Huang, W. –P., & Zhao, W. Self-collimating photonic-crystal wave plates, *Opt. Lett.*, 34: 2676 (2009).

[28] Fan, S., Winn, J. N., Devenyi, A., Chen, J. C., Meade, R. D., & Joannopoulos, J. D. Guided and defect modes inperiodic dielectric waveguides, *J. Opt. Soc. Amer. B, Opt. Phys.*, 12: 1267 (1995).

[29] Luan, P., & Chang,K. Transmission characteristics of finite periodic dielectric waveguides, *Opt. Express*, 14: 3263 (2006).

[30] Lee, K., Chen, C., & Lin, Y. Transmission characteristics of various bent periodic dielectric waveguides, *Opt.Quantum Electron.*, 40: 633 (2008).

[31] Chigrin, D. N., Lavrinenko, A. V., & Torres, C. M. S. Nanopillars photonic crystal waveguides, *Opt. Express*, 12: 617 (2004).

[32] Chigrin, D. N., Lavrinenko, A. V., & Torres, C. M. S. Numerical characterization of nanopillar photonic crystalwaveguides and directional couplers, *Opt. Quantum Electron.*, 37: 331 (2005).

[33] Chigrin, D. N., Zhukovsky, S. V., Lavrinenko, A. V., & Kroha, J. Coupled nanopillar waveguides optical properties andapplications, *Phys. Stat. Sol. (A)*, 204: 3647 (2007).

[34] Zhukovsky, S. V., Chigrin, D. N., & Kroha, J. Low-loss resonant modes in deterministically aperiodic nanopillar waveguides, *J. Opt. Soc. Amer. B, Opt. Phys*., 23: 2265 (2006).

[35] Zhukovsky, S. V., Chigrin, D. N., Lavrinenko, A. V. & Kroha, J. Selective lasing in multimode periodic and non-periodic nanopillar waveguides, *Phys. Stat. Sol. (B)*, 244: 1211 (2007).

[36] Boucher, Y. G., Lavrinenko, A. V., & Chigrin, D. N. Out-of-phase coupled periodic waveguides: A"couplonic"approach, *Opt. Quantum Electron*., 39: 837 (2007).

[37] Sukhorukov, A. A., Lavrinenko, A. V., Chigrin, D. N., Pelinovsky, D. E., & Kivshar,Y. S. Slow-light dispersion in coupled periodic waveguides, *J. Opt. Soc. Amer. B, Opt. Phys.*, 25: C65 (2008).

[38] Bock, P. J., Cheben, P., Schmid, J. H., Lapointe, J., Delâge, A., Janz, S., Aers, G. C., Xu, D.-X., Densmore, A., & Hall,T. J. Subwavelength grating periodic structures in silicon-on-insulator: A new type of microphotonic waveguide, *Opt.Express*, 18: 20251 (2010).

[39] Bock, P. J., Cheben, P., Schmid, J. H., Lapointe, J., Delâge, A., Xu, D.-X., Janz, S., Densmore,A., & Hall,T. J. Subwavelength grating crossings for silicon wire waveguides, *Opt. Express*, 18: 16146 (2010).

[40] Zhang, Y., Huang, W., & Li, B. Fabry–Pérotmicrocavities with controllable resonant wavelengths in periodic dielectric waveguides, *Appl. Phys. Lett.*, 93: 031110 (2008).

[41] Luan P., & Chang, K. Periodic dielectric waveguide beam splitter based on co-directional coupling, *Opt. Express*, 15: 4536 (2007).

[42] Zheng, G., Li, H., Jiang, L., Jia, W., Wang, H. & Li, X. Design of an arbitrarily bent beam splitter for optical interconnections based on co-directional coupling mechanism, *J. Opt. A: Pure Appl. Opt.*, 10: 125303 (2008).

[43] Huang, W., Zhang, Y. & Li, B. Ultracompact wavelength and polarization splitters in periodic dielectric waveguides, *Opt. Express*, 16: 1600 (2008).

[44] Zeng, S., Zhang, Y., & Li, B. Self-imaging in periodic dielectric waveguides, *Opt. Express*, 17: 365 (2009).

[45] Dai, Q. F., Li, Y. W., & Wang, H. Z. Broadband two-dimensional photonic crystal wave plate, *Appl. Phys. Lett.*, 89: 061121 (2006).

[46] Solli, D. R., McCormich, C. F., Chiao, R. Y., & Hickmann, J. M. Experimental demonstration of photonic crystal waveplates, *Appl. Phys. Lett.* 82: 1036 (2003).

[47] Solli, D. R., & Hickmann, J. M. Photonic crystal based polarization control devices, *J. Phys. D: Appl. Phys.*, 37: R263 (2004).

[48] Solli, D. R., McCormich, C. F., & Hickmann, J. M. Polarization-dependent reflective dispersion relations of photonic crystals for waveplate mirror construction, *J. Lightwave Technol.*, 24: 3864 (2006).

[49] Solli, D. R., & Hickmann, J. M. Engineering an achromatic photonic crystal waveplate, *New J. Phys.*, 8: 132 (2006).

[50] Kosaka, H., Kavashima, T., Tomita, A., Notomi, M., Tamamura, O., Sato, T., & Kavakami, S. Self-collimating phenomena in photonic crystals, *Appl. Phys.Lett.* 74: 1212 (1999).

[51] Yu, X. & Fan, S. Bends and splitters for self-collimated beams in photonic crystals, *Appl. Phys. Lett.*, 83: 3251 (2003).

[52] Zabelin, V., Dunbar, L. A., Le Thomas, N., & Houdr, R. Self-collimating photonic crystal polarization beam splitter, *Opt. Lett.*, 32: 530 (2007).

[53] Azami, N., Villeneuve, E., Villeneuve, A., & Gonthier, F. All-SOP all-fibre depolariser, *Electron.Lett.*, 39: 1573 (2003).

IntechOpen

IntechOpen

IntechOpen

IntechOpen